

**EXPERIMENTAL AND THEORETICAL STUDIES
OF (2E,5E)-2,5-BIS(2-METHOXYBENZYLIDENE)CYCLOPENTANONE:
STRUCTURAL, ELECTROCHEMICAL, AND SPECTROSCOPIC FEATURES,
SOLID-STATE INTERACTIONS, MOLECULAR DOCKING, AND ADSORPTION
STUDIES ONTO 2D CARBON NANOMATERIALS**

**Veprim Thaçi^{1,2}, Arianit A. Reka³, Nataša Ristovska¹, Ramiz Hoti¹, Avni Berisha^{1*},
Jane Bogdanov^{2*}**

¹Department of Chemistry, FMNS, University of Prishtina “Hasan Prishtina”, 10000 Prishtina,
Kosovo

²Institute of Chemistry, Faculty of Natural Sciences and Mathematics,
Ss. Cyril and Methodius University in Skopje, 1000 Skopje, N. Macedonia

³Faculty of Natural Sciences and Mathematics, University of Tetovo, Ilinden n.n., 1200 Tetovo,
N. Macedonia

veprim.thaci@uni-pr.edu; avni.berisha@uni-pr.edu; j_b_bogdanov@yahoo.com

A monocarbonyl analog of curcumin, (2E,5E)-2,5-bis(2-methoxybenzylidene)-cyclopentanone (**B2MBCP**), was prepared and characterized via spectroscopic methods (NMR, UV-Vis, FT-IR, and MS). Furthermore, density functional calculations were implemented to study the molecular structure and spectroscopic features, as well as adsorption properties. In addition, Hirshfeld surface and NBO theoretical analysis were carried out. The reduced density gradient (RDG) analysis via non-covalent interactions (NCI) and interaction region indicator (IRI) indicate the presence of extensive Van der Waals interactions. These interactions are classified in different contributions and energy stabilization from Hirshfeld surface analysis where the dominant type of contacts are H···H contacts. The molecular docking studies of **B2MBCP** with DNA revealed cooperative interactions that led to intercalation. The results from the cyclic voltammetry (CV) measurements agreed with the calculated energies of the frontier orbitals and the compound structure. Theoretical studies indicated that the relatively flat **B2MBCP** is adsorbed onto a graphene surface, with a significant adsorption energy of -41.19 kcal/mol. The results of this study provide a better overall picture of the properties of MAC with a cyclopentanone core and can be taken as a useful guide in the search for new biologically active compounds and new possible means of delivery.

Keywords: (2E,5E)-2,5-bis(2-methoxybenzylidene)cyclopentanone; spectroscopic characterization; cyclic voltammetry; DFT; graphene; adsorption; molecular docking; solid-state interactions

**ЕКСПЕРИМЕНТАЛНА И ТЕОРЕТСКА СТУДИЈА
НА (2E,5E)-2,5-БИС(2-МЕТОКСИБЕНЗИЛИДЕН)ЦИКЛОПЕНТАНОН:
СТРУКТУРНИ, ЕЛЕКТРОХЕМИСКИ И СПЕКТРОСКОПСКИ ОДЛИКИ, ИНТЕРАКЦИИ
ВО ЦВРСТА ФАЗА, МОЛЕКУЛСКО ПРИПОЈУВАЊЕ И АДСОРПЦИОНИ ИСПИТУВАЊА
КОН 2D ЈАГЛЕРОДНИ НАНОМАТЕРИЈАЛИ**

Монокарбонилен аналог на куркумин (MAC), (2E,5E)-2,5-бис(2-метоксибензилиден)-циклопентанон (**B2MBCP**), беше синтетизиран и карактеризиран со спектроскопски методи (NMR, UV-Vis, FT-IR и MS). Имплементирани беа DFT-пресметки за проучување на молекуларната структура и спектроскопските карактеристики, како и адсорпционите својства. Дополнително беше извршена теоретска анализа на Хиршфелдовата површина и NBO. Анализата

на редуциран градиент на густина (RDG) преку нековалентни интеракции (NCI) и индикатор за регион на интеракција (IRI) укажува на присуство на екстензивни Ван дер Валсови интеракции. Овие интеракции се класифицирани на различни придонеси и енергетска стабилизација од анализата на Хиршфелдовата површина, каде доминантен тип се $\text{H}\cdots\text{H}$ контактите. Студиите за молекуларно припојување на **B2MBCP** на ДНК открија кооперативни интеракции, што резултира со интеркалирање. Резултатите од цикличната волтаметрија (CV) се согласуваат со пресметаните енергии на граничните орбитали и структурата на соединението. Теоретските студии покажале дека релативно рамниот **B2MBCP** се апсорбира на површината на графен, со значителна енергија на апсорпција од $-41,19$ kcal/mol. Резултатите од оваа студија даваат подобра целокупна слика за својствата на овој MAC со циклопентанонско јадро и можат да се земат како корисен водич во потрагата по нови биолошки активни соединенија и нови можни начини за достава.

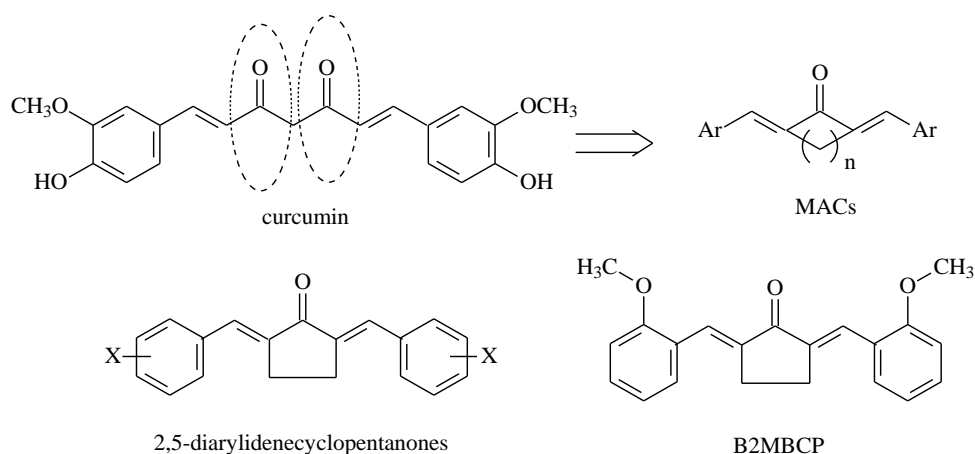
Клучни зборови: (2E,5E)-2,5-бис(2-метоксибензилиден)циклопентанон; спектроскопска карактеризација; циклична волтаметрија; DFT; графен; апсорпција; молекуларно припојување; интеракции во цврста состојба

1. INTRODUCTION

Curcumin is a natural product obtained from the dried rhizome of the plant *Curcuma longa*.¹ Curcumin has been approved as a food additive and is frequently used as a herbal supplement, a coloring agent and flavoring in food, and as a cosmetic ingredient.² Furthermore, it has a wide range of biological activities such as anti-inflammatory, anti-amyloid, anticancer, anti-ischemic, antimicrobial, and antioxidant, among others.³ Curcumin has a number of traditional pharmacological uses in the treatment of ailments, including external/internal wounds, liver disorders, blood purification, antimicrobial activity, and swollen joints.⁴⁻⁶ Curcumin, however, has significant pharmacokinetic drawbacks, including low absorption, rapid metabolism, and the requirement for repeated oral dosages, limiting its use.^{7,8}

The role of curcumin as a lead compound has been controversial, and certain authors classify it as

PAINS (pan-assay interference compounds), as well as an IMPS (invalid metabolic panaceas).⁹ Besides all of the drawbacks mentioned above, curcumin has been a starting point and inspired researchers to make analogs in order to improve the chemical stability and bioavailability. Curcumin is relatively stable at pH values less than 6.5. However, the enolizable 1,3-diketo moiety is the culprit for the low stability at higher pH, including physiological conditions (pH 7.4 and 37 °C). Moreover, the phenolic OH groups are prone to oxidation.¹⁰ One way to circumvent this is to replace the 1,3-diketo functionality with a single ketone but keep the enone system, which is important for bioactivity (Scheme 1). The resulting compounds were named monocarbonyl analogs of curcumin (MACs), and they are based on the 1,5-diaryl-1,4-pentadien-3-one system.¹¹⁻¹⁴ Indeed, these MACs have been shown to have higher stability than curcumin¹⁵, and they have diverse biological activity.^{12,13}



Scheme 1. Removal of the diketo functionality from curcumin leads to more stable monocarbonyl analogs. The biologically active MACs can be acyclic ($n = 0$), with a cyclopentanone core ($n = 2$), a cyclohexanone core ($n = 3$), or a 4-piperidone core. The most conformationally rigid MACs are 2,5-diarylbenzylidencyclopentanones. The structural formula of the title compound is (2E,5E)-bis(2-methoxybenzylidene)cyclopentanone (**B2MBCP**).

Our research groups have been involved in the synthesis and purification of these compounds and methodically exploring their biological activity.^{16–20} For this study we have chosen the symmetrical (2E,5E)-2,5-bis(2-methoxybenzylidene)cyclopentanone (**B2MBCP**), because it has been evident from previous studies that MACs with methoxy and alkoxy groups, but without reactive phenolic OH group, have improved stability and biological activity.^{12,21} The title compound represents the simplest cyclopentanone MAC with methoxy groups in the ortho position, where the influence on the dienone system will be the greatest. Moreover, **B2MBCP** in biological tests exhibited cytotoxicity to human KB cells and was shown to be active after 72 hours against human PC3 cells by MTT analysis. It also has superior hydrolytic stability compared to curcumin and other classes of MACs.¹⁵ Also, according to the study by Zoete et al. it is expected to be potent in inducing the activity of NAD(P)H : quinone reductase (NQO1), a prototypic phase 2 cancer-protective enzyme.²² Here, the potency of the compounds was correlated/ranked with the energy of the HOMO. The general idea was to synthesize and purify **B2MBCP** and carry out more detailed experimental and theoretical investigations with emphasis on its spectroscopic properties, structure, and solid-state interactions.¹⁵

It is necessary to control the electrophilicity and redox characteristics of the Michael acceptor for the optimal biological activity of MAC. For MACs with a cyclopentanone core, there is data for redox potentials of unsubstituted and para-substituted derivatives. Herein, we utilize cyclic voltammetry (CV) using glassy carbon (GC) in acetonitrile solution to obtain valuable electrochemical data. These measurements were made to see the effect of orthomethoxy substituents on the benzene rings of the cross-linked dienone on the redox potentials and also to examine the energy and other features of the frontier orbitals of the molecule.²³

Graphene is a pure form of carbon with a two-dimensional structure, which makes it highly appealing and provides a large surface area for adsorption. Graphene has shown excellent absorbent properties for flat conjugated organic compounds through Van der Waals forces and π - π stacking interactions.^{24,25} Graphene and graphene oxide have a high selectivity surface area for specific molecules due to their unique electronic structures.²⁶ This will be a preliminary study to explore the efficiency of the adsorption utilizing a solution of **B2MBCP** in organic solvent(s).

Furthermore, it is interesting to note that the experimental and theoretical studies of the interac-

tion/binding of MAC to DNA are scarce.²⁷ From the experimental in vitro study by Huber et al., it was established that there was no DNA binding of 4-piperidone and cyclohexanone MACs. However, the “flattest” cyclopentanone analogs were not investigated.

Herein, we would like to present our theoretical and experimental studies of the title compound (**B2MBCP**) regarding structural, spectroscopic, and electrochemical features, solid-state interactions, and adsorption on graphene. Additionally, its interaction with DNA may be relevant to its biological activity, which was probed via a molecular docking study with DNA.

2. EXPERIMENTAL SECTION

2.1. Reagents and instruments

Cyclopentanone (99.8%), benzaldehyde (98%), and 2-methoxybenzaldehyde (98%) were obtained from Sigma Aldrich. Methanol (99.9%, Chromasolv HPLC grade), dichloromethane, chloroform, carbon tetrachloride, ammonium chloride, and sodium hydroxide were obtained from Merck. All chemicals were used without further purification. The progress of the reactions was monitored by thin-layer chromatography (TLC) plates, which were aluminum sheets pre-coated with silica gel containing fluorescent indicator (Merck, Kieselgel 60, F₂₅₄). The plates were visualized by direct inspection (yellow spots) or by using a Camag UV lamp (254 nm and 266 nm). Melting points were determined using a Buchi B-545 melting-point apparatus. Infrared spectra were recorded on an FT-IR, Shimadzu 8400s and Agilent Cary 630. The IR absorption spectra were recorded on a Perkin-Elmer System 2000 FTIR spectrometer with the KBr pellet technique. The spectra were recorded with a resolution of 4 cm⁻¹, using 32 scans. The solution spectra (CH₂Cl₂ or CCl₄) were recorded in a sealed cell for liquids (SLC) with KBr windows, with a path length of 0.024 mm (conc. of **B2MBCP** of 30 mg/ml). The ATR spectra were recorded on the same Agilent Cary 630 FTIR spectrometer using a diamond ATR accessory. ¹H and ¹³C NMR spectra were obtained on a Bruker Avance 400 MHz spectrometer (at 400 and 100 MHz, respectively) in d₆-chloroform solvent with tetramethylsilane (TMS) as an internal standard. Chemical shifts were measured relative to TMS or the residual solvent in CDCl₃. The UV-Vis spectra were recorded on a Helios Alpha Spectrophotometer in CCl₄ and CH₂Cl₂ solvents. The mass spectral measurements were carried out on an Agilent 1100

HPLC system equipped with an atmospheric-pressure chemical ionization (APCI) interface and an ion-trap mass analyzer (G2445A Spectrometer) controlled by LCMSD software (Agilent, v.4.1). Mass spectral data were acquired in the positive ionization mode. The full scan covered the mass range of 15–600 m/z . Electrochemical measurements were performed with the PalmSens BV device, version 5.9, with the cyclic voltammetry method in a closed cell deaerated with N_2 gas using a three-electrode system. A glassy carbon electrode was used as the working electrode. An Ag/AgCl electrode (saturated KCl) was the reference electrode, and a graphite electrode was the counter electrode. The measurements were performed after dissolving the compound in acetonitrile at a concentration of 1 mmol and in the presence of the basic electrolyte TBAHPh with a concentration of 0.1 M, degassing every 5 min with nitrogen gas, and in the potential range -1.6 to 1.8 V.

For the determination of adsorption onto graphene, first, a 100 cm^3 solution was prepared with a concentration of 100 ppm (100 mg/dm^3) using acetonitrile as the solvent. The concentration of the compound was kept unchanged at 100 ppm (it was diluted 10 times to avoid errors because it had an absorbance higher than 2), while the amount of graphene was changed to 10, 25, and 50 mg. The solutions were stirred for 24 h with a magnetic stirrer at 700 rpm, then filtered with a $45\text{ }\mu\text{m}$ nylon membrane prior to UV-Vis measurement ($\lambda_{\text{max}} = 380\text{ nm}$). The residual concentration measurement was determined by UV-Vis. The UV-Vis spectra were recorded on a Helios Alpha Spectrophotometer using a quartz cuvette.

2.2. Synthesis of (2E,5E)-bis(2-methoxybenzylidene)cyclopentanone (B2MBCP)

The title compound was prepared by adaptation of the procedure described by Hadzi Petrusse et al.¹⁶ Cyclopentanone (0.6309 g, 10 mmol) and 2-methoxybenzaldehyde (2.042 g, 15 mmol), followed by methanol (10 ml), were added to a round-bottomed flask (25 ml) equipped with a condenser. The solution was stirred at ambient temperature for 5 min. Afterward, a 20% (w/v) aqueous solution of sodium hydroxide (2.0 ml) was added dropwise over a 5 min period. Initially, the reaction mixture turned yellow, and after a few minutes, a yellow precipitate appeared. The reaction mixture was stirred for an additional 50 min at ambient temperature. The reaction mixture was cooled at $0\text{ }^\circ\text{C}$ for 10 min, then 5 ml of water was added. The resulting yellow suspension was filtered on a Büchner

funnel. The yellow solid was washed with saturated aqueous ammonium chloride solution ($1 \times 10\text{ mL}$), distilled water ($3 \times 10\text{ mL}$), and ice-cold methanol (5 ml). The yellow solid obtained was dried *in vacuo*. Recrystallization from a methanol/chloroform mixture was carried out as described in the literature,²⁸ giving 1.680 g (53%) of **B2MBCP** as yellow crystals. mp $176.6\text{--}178.4\text{ }^\circ\text{C}$ (mp $150\text{--}152\text{ }^\circ\text{C}$, lit.¹⁵; $155\text{ }^\circ\text{C}$, lit.²⁹); R_f (4:1 *n*-hexane/EtOAc) = 0.32; $^1\text{H NMR}$ (400 MHz, chloroform-*d*): δ 7.68 – 7.55 (m, 6H), 7.49 – 7.41 (m, 4H), 7.38 (dd, $J = 8.4, 6.2\text{ Hz}$, 2H), 3.13 (s, 4H). $^{13}\text{C NMR}$ (100 MHz, chloroform-*d*): δ 196.22, 158.90, 137.63, 130.67, 129.77, 127.99, 125.03, 120.23, 110.81, 55.52, 26.84; FT-IR (KBr): 1677 cm^{-1} (m, C=O), FT-IR (ATR): 1678 cm^{-1} (m, C=O), FT-IR (SLC with CCl_4): 1698 cm^{-1} (m, C=O) and FT-IR (SLC with CH_2Cl_2): 1692 cm^{-1} (m, C=O). UV-Vis (CCl_4): $\lambda_{\text{max}} = 367\text{ nm}$, $\epsilon = 31980\text{ M}^{-1}\text{cm}^{-1}$; (CH_2Cl_2): $\lambda_{\text{max}} = 371\text{ nm}$, $\epsilon = 35307\text{ M}^{-1}\text{cm}^{-1}$; MS-APCI (m/z) = 321 (MH^+).

2.3. Theoretical calculations

The molecular structure of (2E,5E)-2,5-bis(2-methoxybenzylidene)cyclopentanone (*in vacuo* and solvent) was optimized using density functional theory (DFT) and B3LYP functional using 6-31+G(d,p) basis set via the Gaussian 16 software. The B3LYP functional,³⁰ which employs Becke's three-parameter hybrid exchange functional and the Lee-Yang-Parr correlation functional, has been used effectively to assess the characteristics of numerous organic compounds.^{31,32} The vibrational frequencies of the optimized geometries were validated.^{33,34} The excited-state geometry of **B2MBCP** was optimized using TD-DFT with the same functional and basis set. In all calculations, the solvent effect was considered a polarizable continuum model (PCM) using the integral equation formalism variant (IE-FPCM). The non-covalent interaction (NCI) analysis was performed using Multiwfn software, and the NCI surface³⁵ was plotted using Visual Molecular Dynamics software.^{36,37}

All calculations based on density-functional-based tight-binding (DFTB) were executed using the software tool known as DFTB+.^{38,39} This software package is widely used for conducting quantum mechanical simulations of various types of materials, including solids, insulators, metals, and biological systems. The DFTB+ software tool is highly efficient and enables rapid computation of large systems while being significantly faster than the *ab initio* methods. It also offers several advantages such as the ability to model

chemical reactions, predict molecular properties, and simulate reactions in complex environments. The 3OB-Koster library set was used to compute the likelihood of interaction and collision between pairs of C, N, O, H, and S. For the calculations, the convergence tolerance for energy was 0.01 kcal/mol, for force it was 0.1 kcal/mol, and the displacement was 0.001.

CrystalExplorer 17.5 was used to generate Hirshfeld surfaces and their associated two-dimensional fingerprint maps. The normalized contact distance (d_{norm}) was calculated using both d_e (distance from the point to the nearest nucleus external to the surface) and d_i (distance from the point to the nearest nucleus external to the surface). The combination of d_e and d_i in the form of a two-dimensional fingerprint plot offers an overview of a crystal's intermolecular interactions. Interaction energies in the molecule were calculated using CE-B3LYP/6-31G(d,p) quantum level of theory, as available in CrystalExplorer 17.5.

3. RESULTS AND DISCUSSION

3.1. ^1H and ^{13}C NMR spectroscopy

The title compound was prepared by a Claisen-Schmidt reaction and purified by recrystallization from a 5:1 chloroform/methanol mixture. Based on the NMR spectroscopic data and comparison with the literature²⁹, it can be concluded that **B2MBCP** is a symmetric molecule and has *E,E* stereochemistry. This stereochemical assignment is supported by the crystallographic data.²⁸ In ^1H NMR, the protons of the CH_2 groups from the cy-

clopentanone ring appear at 3.00 ppm, whereas the protons from the methoxy groups appear as a singlet at 3.87 ppm. The olefinic protons from the dienone system appear as a singlet at 8.00 ppm. There are 8 aromatic protons, and their splitting and coupling correspond to a 1,2-disubstituted benzene (Fig. 1). There are 11 peaks in the ^{13}C NMR broadband decoupled spectrum, which confirms the symmetric structure. The carbonyl group appears at 196.27 ppm. There are 8 olefinic and aromatic carbons; the carbon from the methoxy group appears at 55.55 ppm, and the CH_2 group from the cyclopentanone moiety is at 26.87 ppm. The ^{13}C NMR spectrum was also simulated via calculation, and the experimental and theoretical values are in good agreement (Table 2). The conjugated nature of the compound and the dienone system is confirmed by UV-Vis spectra and IR data (sections 3.2 and 3.3). Similarly, ^{13}C NMR spectra (Figure 2) agree with the (2*E*,5*E*)-2,5-bis(2-methoxybenzylidene)cyclopentanone structure and the previously reported data.

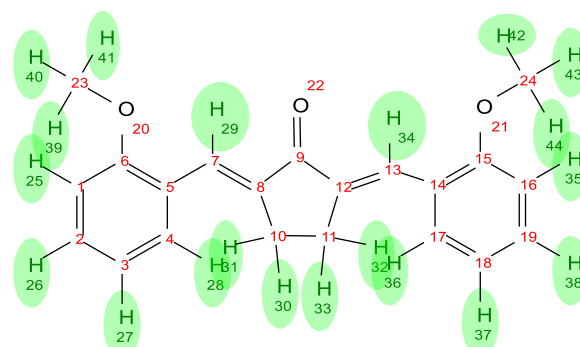


Table 1

Theoretical and experimental ^1H and ^{13}C spectra of **B2MBCP**.
Chemical shifts are given relative to TMS, and all values are given in ppm.

^{13}C NMR			^1H NMR		
Atoms	Exp. (ppm)	Theor. (ppm)	Atoms	Exp. (ppm)	Theor. (ppm)
C9 (C=O)	196.27	197.25	H29, H34	8.00 (s)	7.73 (s)
C6, C15	158.94	158.99	H28, H36	7.52 (dd)	7.51 (dd)
C8, C12	137.66	140.43	H26, H38	7.34 (ddd)	7.41 (ddd)
C7, C13	130.71	135.67	H27, H37	6.99 (td)	7.19 (td)
C2, C19	129.81	133.06	H25, H35	6.92 (dd)	6.98 (dd)
C4, C17	128.02	130.21	H39, H40, H41, H42, H43, H44	3.87 (s)	3.84 (s)
C5, C14	125.07	126.15	H30, H31, H32, H33	3.00 (s)	2.96 (s)
C3, C18	120.26	123.22			
C1, C16	110.84	113.55			
C23, C24 (O-CH3)	55.55	55.39			
C10, C11 (CH2)	26.87	26.70			

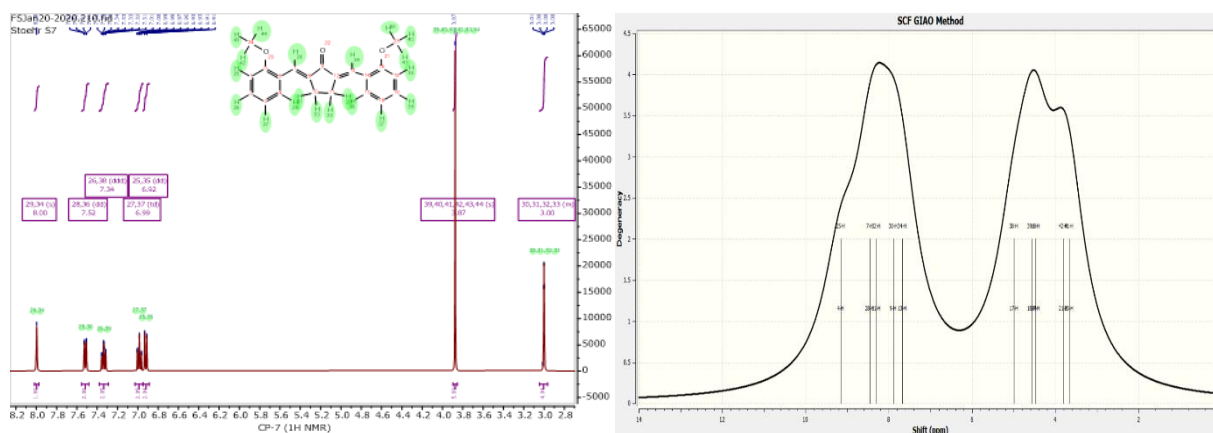


Fig. 1. ¹H-NMR spectrum of synthesized **B2MBCP** obtained in CDCl₃ (400 MHz) (left) and the calculated ¹H-NMR spectrum of **B2MBCP** (right)

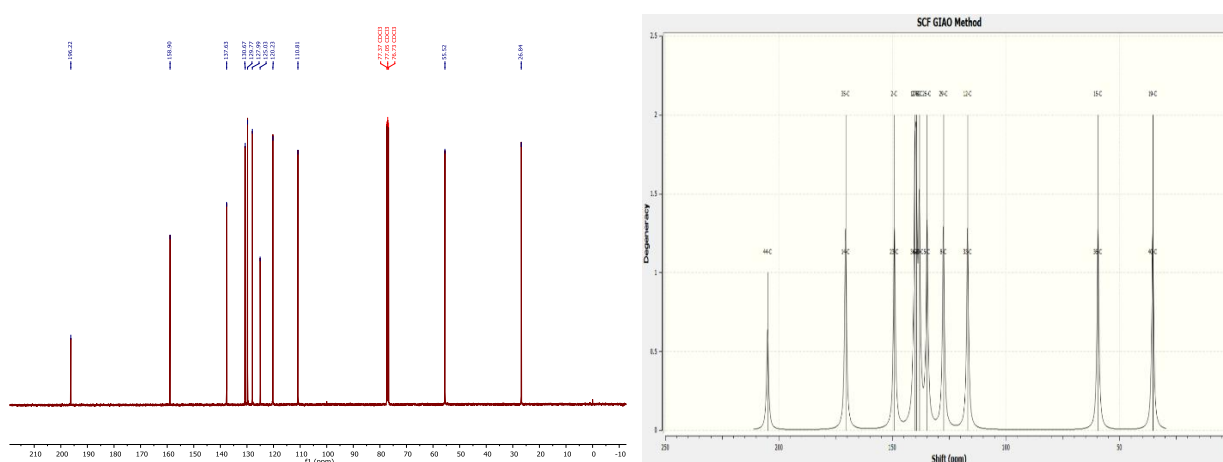


Fig. 2. ¹³C-NMR spectrum of the synthesized **B2MBCP** (left) and calculated ¹³C NMR spectrum (right)

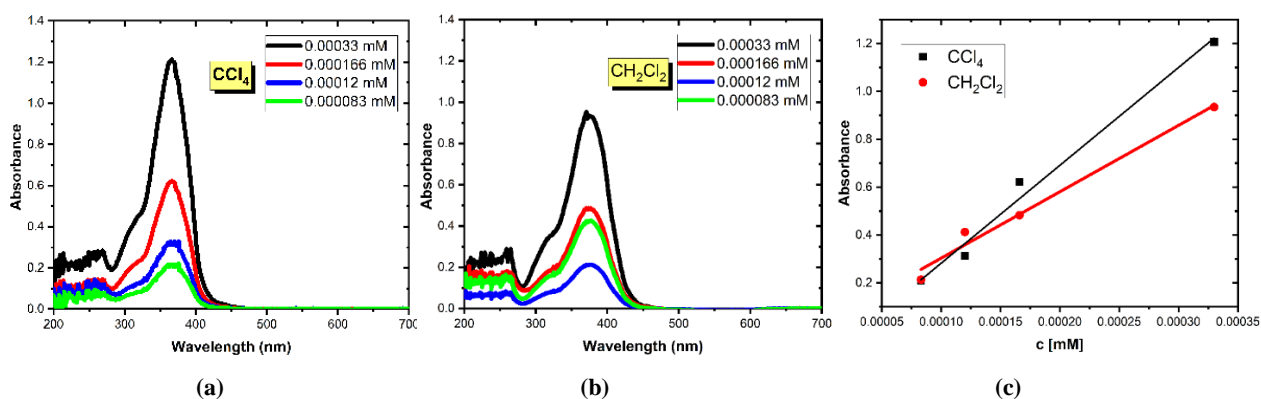


Fig. 3. UV-Vis spectra of **B2MBCP** in CCl₄ (a) and CH₂Cl₂ (b) and absorbance vs. concentration plots for determining the molar absorptivity (c)

3.2. UV-Vis spectroscopic studies

To get molecular insight into these compounds, UV-Vis absorption spectra were obtained in CCl₄ and CH₂Cl₂ (200–800 nm) and compared to the computed spectra using time-dependent density

functional theory (TDDFT). The graphs of the calculated spectra are depicted in Figure 3. The calculated UV-Vis spectra agree with those obtained experimentally. This compound had an absorption maximum at 364 nm in CCl₄ and at 371 nm in dichloromethane.

The compound has moderate molar extinction coefficients (ϵ) with a value of $31980 \text{ M}^{-1}\text{cm}^{-1}$ in CCl_4 and $35307 \text{ M}^{-1}\text{cm}^{-1}$ in CH_2Cl_2 . These absorptions, as evidenced in previous similar compounds, are due to $\pi \rightarrow \pi^*$ transition at a lower wavelength (presented as a shoulder at 312 nm) and $n \rightarrow \pi^*$ at higher ones.⁴⁰ It was observed that the long wavelength absorption band (LAB) is sensitive to the polarity of the solvent, where the λ_{max} shifts to higher wavelengths as the polarity of the solvent increases (364 nm (CCl_4), 371 nm (CH_2Cl_2), 378 nm (CH_3CN)). This is another confirmation that the LAB arises from the $n \rightarrow \pi^*$ transition, which is known to be sensitive to solvent polarity.

3.3. Vibrational spectroscopy (FT-IR)

Considering the calculated wavenumbers, the assignments of the molecule's vibrational wavenumbers were interpreted by comparing with similar molecules^{41–43} and expressed in terms of the

total energy distribution (TED) values. Also, theoretical vibration wavenumbers of **B2MBCP** were calculated at the same level theory with 6–31G(d,p) as the basis set. The calculated vibrational wavenumbers of the free form and the dissolved form of the molecule (in CCl_4 and CH_2Cl_2 solutions and solid-state). Also, experimental wavenumbers of the spectrum of solid samples (ATR) and dissolved forms of (2E,5E)-2,5-bis(2-methoxybenzylidene)cyclopentanone are given in Figure 4. They show the experimental and theoretical infrared spectra of the solid phase and solvation forms of 2,5-bis(2-methoxybenzylidene)cyclopentanone, respectively. From the experimental data, it can be concluded that the key C=O group is conjugated, which agrees with NMR and UV-Vis data. The C=O stretching vibration in the solid sample (ATR technique) was observed at 1675 cm^{-1} , at 1692 cm^{-1} in CH_2Cl_2 solution, and in the least polar solvent (CCl_4) at 1698 cm^{-1} . The same trends were observed in the calculated IR spectra.

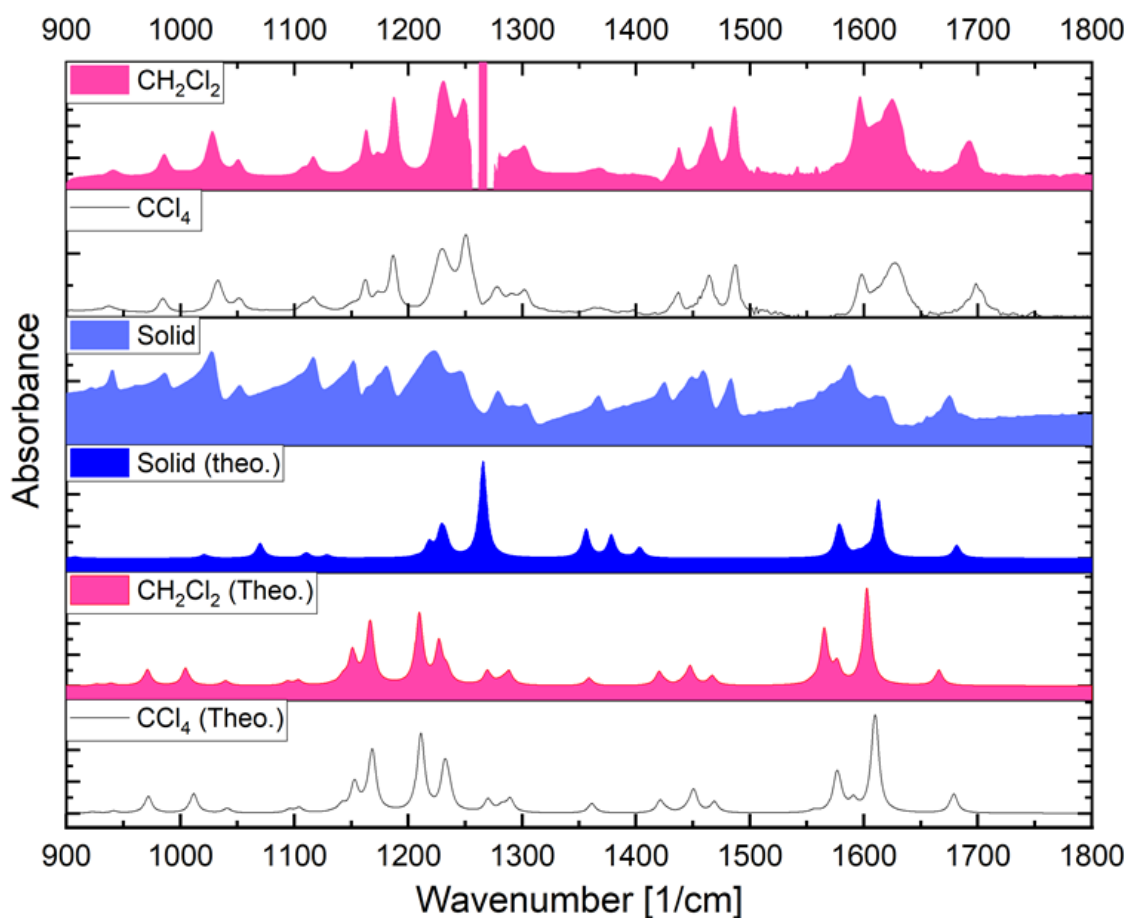


Fig. 4. Theoretical and experimental FTIR spectra of (2E,5E)-bis(2-methoxybenzylidene)cyclopentanone in different media: solid state, CCl_4 , and CH_2Cl_2

Table 2

Theoretical and experimental IR spectra of **B2MBCP**. Displacements of C=O and C-O-C groups in relation to the solid state and the influence of CCl₄ and CH₂Cl₂ solutions with values given in cm⁻¹

Modes	Solid	Solid (theo.)	CH ₂ Cl ₂	CH ₂ Cl ₂ (theo.)	CCl ₄	CCl ₄ (theo.)
C=O	1675 cm ⁻¹ str. 939 cm ⁻¹ rock and wag	1613 cm ⁻¹ str. 1022 cm ⁻¹ rock and wag	1692 cm ⁻¹ str. 941 cm ⁻¹ rock and wag	1665 cm ⁻¹ str. 971.68 cm ⁻¹ rock and wag	1698 cm ⁻¹ str. 936 cm ⁻¹ rock and wag	1677 cm ⁻¹ str. 971 cm ⁻¹ rock and wag
C-O-C	1280 cm ⁻¹ strong asym- metric. and 1053 cm ⁻¹ very weak asymmetric.	1265 cm ⁻¹ strong asymmet- ric. and 1069 cm ⁻¹ very weak asymmet- ric.	1249 cm ⁻¹ strong asym- metric. and 1051 cm ⁻¹ very weak asymmetric.	1287 cm ⁻¹ strong asymmetric. and 1151 cm ⁻¹ very weak asymmetric.	1279 cm ⁻¹ strong asym- metric. and 1051 cm ⁻¹ very weak asymmetric.	1289 cm ⁻¹ strong asym- metric. and 1013 cm ⁻¹ very weak asymmet- ric.

3.4. Cyclic voltammetry (CV)

Electrochemical properties of **B2MBCP** were studied by cyclic voltammetry (CV) on a cleaned

surface of glassy carbon (GC) electrodes in acetonitrile solvent (Fig. 5, Table 3). The CV curves were recorded from 0 V to the anodic (-1.6V) or cathodic (+1.6V) region of potentials.^{23,44}

Table 3

Electrochemical potentials of compound **B2MBCP** in acetonitrile measured relative to Ag/AgCl/KCl (sat.) by cyclic voltammetry (CV) in the presence of 0.1 M TBAHPh on glassy carbon (GC) electrode with the potential sweep speed 100 mV s⁻¹.

Compound	E _{red} (V)	I _{red} (μA/V)	ΔE _{red} * (mV)	E _{ox} (V)	ΔE _{ox} ** (mV)	ΔE=E _{ox} -E _{red} (V)
B2MBCP	-1.417	-131.35	3.565	1.467	0	2.884

*shift of reduction potential relative to B2MBCP

**shift of oxidation potential relative to B2MBCP

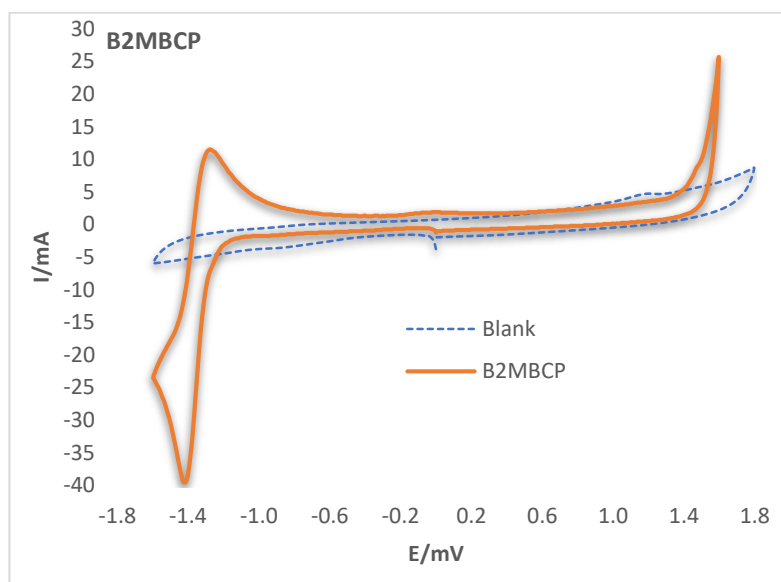


Fig. 5. Cyclic current-potential curves of (2*E*,5*E*)-bis-(2-methoxybenzylidene)cyclopentanone (**B2MBCP**) (a) blank in MeCN (dashed blue line) on glassy carbon (GC) electrode, (b) **B2MBCP** in MeCN (solid orange line) on GC electrode. Both were carried out with potential sweep speed of 100 mV s⁻¹.

The reduction potential (-1.417 V) and the current measured in the potential range of -1.6 to $+1.6$ V indicate the potential at which the studied compound undergoes reduction at the working electrode. The compound was dissolved in MeCN and showed an adsorption in the potential region -1.6 to $+1.6$ V.²³ The experimental data indicates that the **B2MBCP** cathodic peaks in this study are electrochemically irreversible, which corresponds to the transfer of one electron. This finding is in agreement with previously reported findings for related MACs.^{23,45} The electron transfer to the conjugated system of the π -bonds of the substrate (in E1) is mainly localized on the oxygen atom of the carbonyl group. The anion radical formed most likely dimerizes or undergoes protonation (ECE mechanism) with the formation of a free radical, which, as a rule, undergoes reduction at E1 of the substrate.⁴⁴ If one compares the experimental results to the previously reported ones for the para-substituted analog ((2E,5E)-bis-(4-methoxybenzylidene)cyclopentanone), **B4MBCP**, they are quite close. The reduction potential (E_{red}) for **B4MBCP** is -1.39 V, the oxidation potential (E_{ox}) is 1.48 V, and ΔE is 2.87 V.

3.5. Adsorption properties of graphene. Synthesis of graphene

Graphene oxide was prepared by oxidizing graphite with potassium permanganate (KMnO_4) and sulfuric acid (H_2SO_4). This oxidation method forms graphene oxide by creating several oxygen-containing functional groups on graphene flakes.⁴⁶ The graphene oxide suspension was rinsed many times with distilled water after oxidation to eliminate acids and salts. Membrane filtering of the solution yields solid graphene oxide powder. The oxidizing agent type and concentration, reaction duration, temperature, and reaction mixture pH affect graphene oxide quality and characteristics.^{24,47}

Chemical reduction of graphene oxide is a popular way to make high-quality graphene. The oxygen-containing functional groups in graphene oxide must be removed chemically to restore its sp^2 hybridization of carbon atoms. This is done with ascorbic acid. After chemical reduction, graphene has little oxygen and good electrical and mechanical characteristics. Chemically reduced graphene quality varies depending on the kind of reducing agent, concentration, reaction time, reaction mixture temperature, and pH.⁴⁸

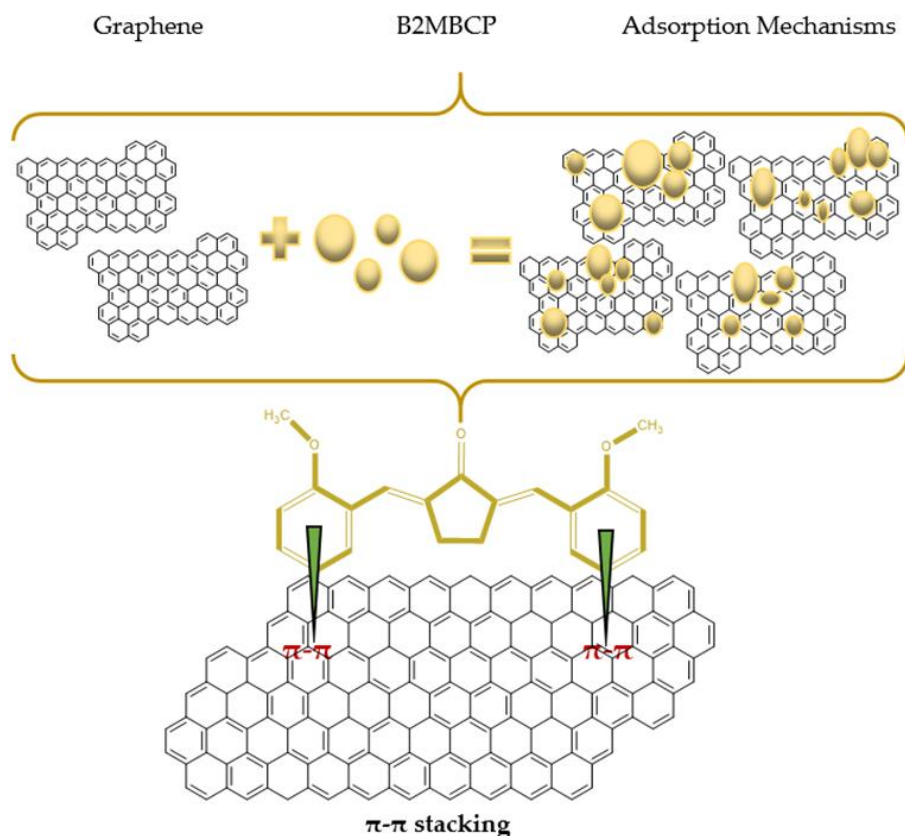


Fig. 6. The interaction mechanism between graphene and the yellow-colored title compound, **B2MBCP**

The adsorption was performed using a specific adsorption mass (10, 25, and 50 mg) of graphene (G) or graphene oxide (GO_x). The solution was stirred for 24 h and afterwards was centrifuged and filtered (45 μm a nylon membrane prior to UV-Vis measurement (λ_{max} = 380 nm)). Based on the UV-Vis assay, graphene was superior to graphene oxide (GO_x) with maximum adsorption effects of 96.35 % compared to 37.9 %. These results align with previous scientific reports on other organic compounds,⁴⁹ and graphene can potentially be used as a biocompatible carrier for biologically active MACs.

3.6. Density-functional-based tight-binding + (DFTB+) calculations

As mentioned before, the DFTB+ software tool is considered a useful and reliable computational tool for performing theoretical calculations.

$$E_{\text{ads}} = E_{\text{Graphene/molecule}} - [(E_{\text{Graphene}}) + (E_{\text{molecule}})] \quad (\text{eq. 1})$$

where $E_{\text{Graphene/molecule}}$ represents the total energy of the interacting system, E_{Graphene} represents the energy of a clean graphene surface, and E_{molecule} represents

the energy of an isolated molecule. Under this notion, a negative value of E_{ads} fits a virtually stable adsorbate–substrate system.

Based on previous work,^{49,52,53} the following equation was used to calculate the adsorption energies (E_{ads}) for all systems:

Table 4

DFTB+ derived parameters and the interaction energy for graphene and B2MBCP

Parameter	Molecule (B2MBCP)	Graphene model	Graphene@molecule
HOMO [eV]	-5.4028	-4.4061	-4.3733
LUMO [eV]	-2.8119	-4.3533	-4.3217
ΔE [eV]	2.59	0.052	0.0516
Energy [kcal/mol]	-33334.4252377	-82650.6062284	-116026.229857
Adsorption energy [kcal/mol]		-41.198	

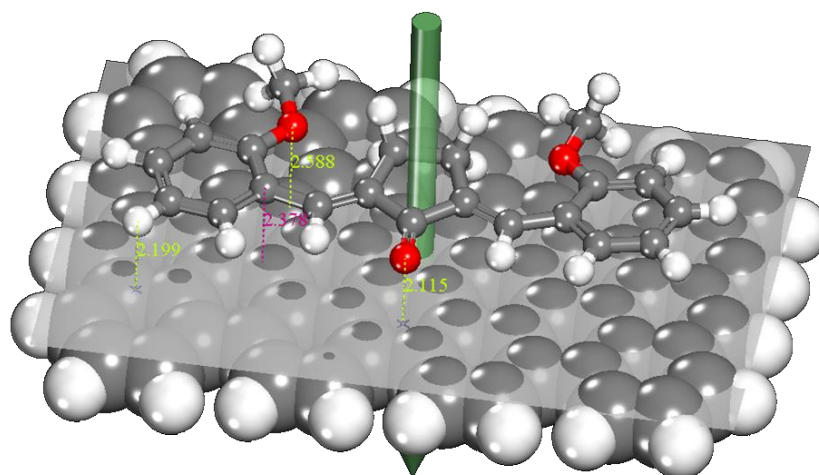


Fig. 7. Optimized geometry and the corresponding mean surface plane of graphene to atom distances of the adsorbed (2E,5E)-2,5-bis(2-methoxybenzylidene)cyclopentanone. As assessed through the analysis of relatively short distances, this surface “closeness” of the adsorbate supports the relatively high adsorption energies.

As represented in Figure 7, the (2E,5E)-2,5-bis(2-methoxybenzylidene)cyclopentanone is spontaneously flat and adsorbed onto the graphene surface, with the significant adsorption energy of -41.19 kcal/mol. These promising results indicate that graphene can be used for the removal of **B2MBCP** from solution(s), or it can be used as a potential carrier of **B2MBC** in biomedical applications.

3.7. Frontier molecular orbital analysis

Generally, the highest occupied molecular orbital (HOMO) and the lowest unoccupied molecular orbital (LUMO) are referred to as frontier molecular orbitals.^{54,55} The HOMO-LUMO energy gap (E_g) indicates that the molecule is quite stable. The LUMO directly senses the molecule's capacity to acquire an electron, whereas the HOMO symbol denotes the molecule's ability to give an electron.⁵⁶

In the title compound, the HOMO orbital is located over the entire structure, and LUMO orbital is mainly dispersed in the central cyclopentanone moiety (Figure 8). Using Koopman's theorem, the energy gap (E_g) of a molecule (3.565 eV) reflects the stability, chemical activity, softness, hardness, chemical potential, electronegativity, and electrophilicity index.⁵⁷ The relatively high dipole moment value indicates that the title chemical is

amenable to additional interactions with other systems.

A summary of all global reactivity parameters is given in Table 5. The negative value of chemical potential indicates that the molecule is stable, while the high value of chemical hardness indicates that the title compound is less reactive and more stable. Due to the compound's high electrophilicity index, it is suitable for biological activity.⁵⁸

Table 5

Calculated parameters of the title compound

Theoretical parameters	
HOMO	-5.8360
LUMO	-2.2710
$\Delta E(\text{HOMO-LUMO})$	3.565
Dipole moment (D)	1.813
Ionization energy (I)	5.8360
Electron affinity (A)	2.2710
Electronegativity (X)	4.0535
Global hardness (η)	1.7825
Chemical potential (π)	-4.0535
Global softness (σ)	0.5610

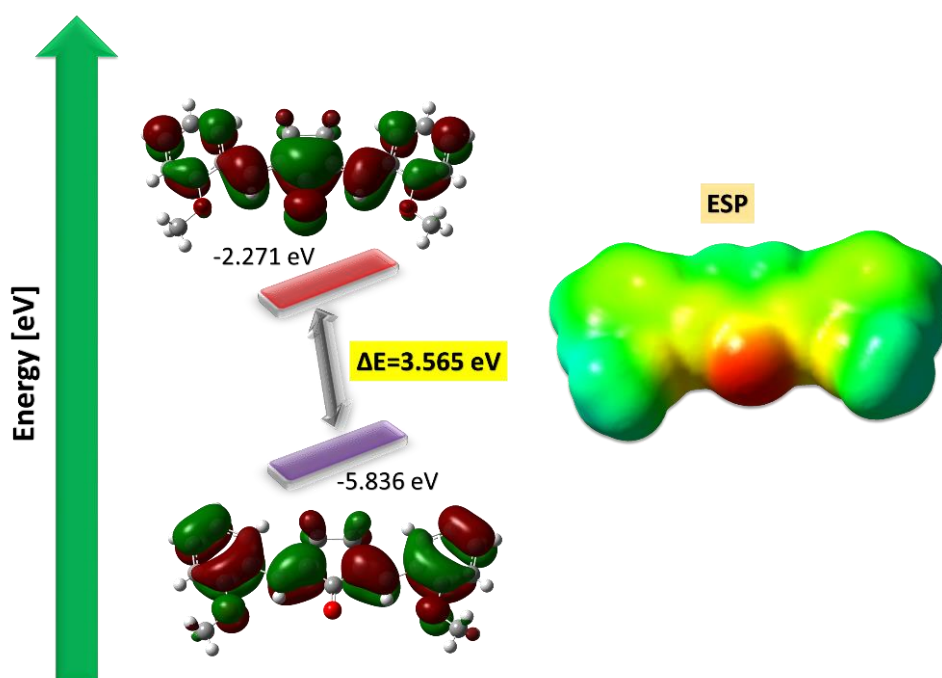


Fig. 8. Optimized structure, HOMO, LUMO and ESP for (2E,5E)-2,5-bis(2-methoxybenzylidene)cyclopentanone using the B3LYP/6-311+g(d,p) plus empirical dispersion=gd3 method

3.8. Hirshfeld surface (HS) analysis

The Hirshfeld surface (HS) divides crystal space into regions for a molecule and its adjacent molecules. In a crystal, ^{59,60} fingerprint intermolecular interactions can be studied using the HS's spatial separation. HS analysis can reveal and quantify non-covalent interactions that stabilize crystal packing. HS d_{norm} , electrostatic potential, shape index, and curvature can be mapped. The d_{norm} property is symmetrical and depends on the van der Waals radii of nuclei inside and outside the Hirshfeld surface (d_i and d_e). Red and blue sections on the d_{norm} represent shorter and longer inter contacts, respectively, while white represents the contact around the Van der Waals radii. Two-dimensional fingerprint plots reveal important crystal intermolecular interactions. HS analysis has

become a powerful tool for understanding intermolecular interactions that affect crystal packing. Over shape index and curvedness, Hirshfeld surfaces show C—H $\cdots\pi$ and π – π intermolecular interactions.⁶¹

Energy framework analysis was used to investigate the energies of intermolecular interactions between the molecules in cluster 3.8. These computations were carried out with Crystal Explorer 17.5 with the basis set B3LYP/6-31. The cylinder's radius is related to the amount of the interaction energy in a given direction.⁶²

The overall fingerprint plot for the molecule is shown in Figure 9. Those decomposed into H \cdots H, H \cdots C/C \cdots H, H \cdots O/O \cdots H, and C \cdots O/O \cdots C contacts illustrated in the same figure together with their relative contributions to the Hirshfeld surface (bottom right).

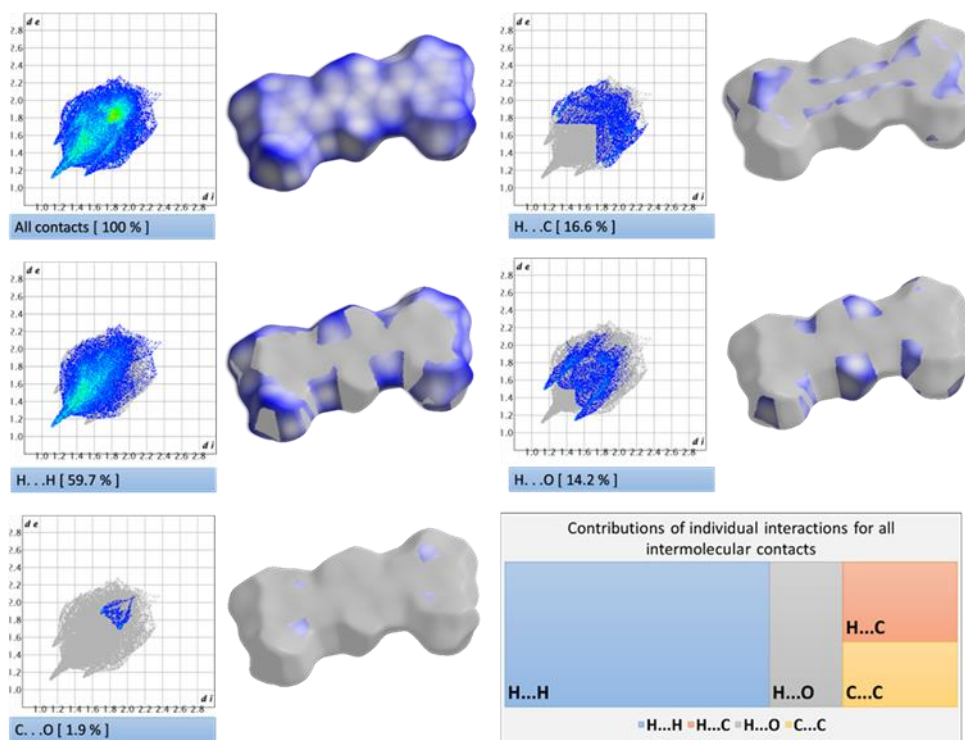


Fig. 9. Two-dimensional fingerprint plots for all intermolecular contacts in the molecule.

Contributions of individual interactions: H \cdots H, H \cdots C/C \cdots H, H \cdots O/O \cdots H, and C \cdots O/O \cdots C.

The outline of the full fingerprint plot is shown in grey. Surfaces to the right highlight the relevant d_{norm} surface patches associated with the specific contacts. The percentage of contribution is specified for each contact

The most prominent type of contacts in the structure corresponds to H \cdots H contacts; they contribute 59.7 % to the overall surface contacts. The presence of C—H $\cdots\pi$ interactions gives rise to a pair of characteristic wings in the fingerprint plot decomposed into C \cdots H/H \cdots C contacts contributing 16.6 % to the Hirshfeld surface. Short

O \cdots H/H \cdots O contacts contribute 14.2 % to the HS and form a pair of spikes.

Koenderink's useful curvature measures, curvedness and shape index,⁶³ provide additional chemical insight into molecular packing. A flat area is defined as a surface with a low curvedness, which may be suggestive of π – π stacking in the crystal. On the other hand, a Hirshfeld surface with a high de-

gree of curvature is shown by dark-blue edges, indicating the lack of π - π stacking.⁶⁴ The shape index is a qualitative measure of shape that is very sensitive to tiny changes in the form of a surface, especially in a flat region. Two sign-differentiated shape indices depict complimentary “bumps and hollows”. The blue bump form with a shape index of more than 1 represents a donor, while the red hollow shape with an index of less than 1 represents an acceptor of intermolecular interaction.

Interaction energies in the molecule were calculated using CE-B3LYP/6-31G(d,p) quantum level of theory, as available in CrystalExplorer 15. The total intermolecular interaction energy (E_{tot}) is the sum of four energy terms: electrostatic (E_{ele}), polarization (E_{pol}), dispersion (E_{disp}) and exchange-repulsion (E_{rep}) with scale factors of 1.057, 0.740, 0.871 and 0.618, respectively⁶⁵. The interaction energies between different molecular pairs are separated into the corresponding coulomb, dispersion, and total energy.⁶⁶ The differences in the strengths of interactions between the molecular pair are given in Table 6.

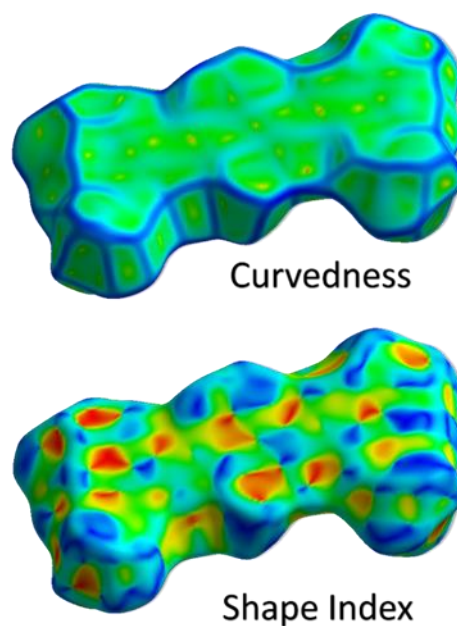


Fig. 10. Calculated Curvedness and Shape index for the (2E,5E)-2,5-bis(2-methoxybenzylidene)cyclopentanone using Crystal Explorer 17.5

Table 6

Interaction energy (kJ/mol) of the molecule

N	Symop	R	Electron density	E_{ele}	E_{pol}	E_{dis}	E_{rep}	E_{tot}
2	-x+1/2, -y+1/2, -z	10.39	B3LYP/6-31G(d,p)	-19.9	-6.3	-19.4	13.5	-34.3
2	x+1/2, y+1/2, z	11.80	B3LYP/6-31G(d,p)	-2.7	-1.0	-11.8	5.7	-10.3
1	-x, -y, -z	3.83	B3LYP/6-31G(d,p)	-14.7	-7.3	-110.3	57.6	-81.5
1	x, y, z	15.28	B3LYP/6-31G(d,p)	6.5	-0.6	-14.3	0.0	-6.1
1	-x, -y, -z	16.56	B3LYP/6-31G(d,p)	1.2	-0.4	-8.2	0.0	-6.2
0	-x+1/2, -y+1/2, -z	10.73	B3LYP/6-31G(d,p)	-0.7	-0.3	-15.1	7.6	-9.4

Scale factors for benchmarked energy models

Energy model	k_{ele}	k_{pol}	k_{disp}	k_{rep}
CE-HF ... HF/3-21G electron densities	1.019	0.651	0.901	0.811
CE-B3LYP ... B3LYP/6-31G(d,p) electron densities	1.057	0.740	0.871	0.618

The relative strengths of interaction energies in individual directions are represented by cylinder-shaped energy frameworks (Fig. 11). Insignificant contacts weaker than a threshold energy of

10 kcal/mol have been omitted from the original figure for clarity. Dispersion forces play the dominant role in the molecule.

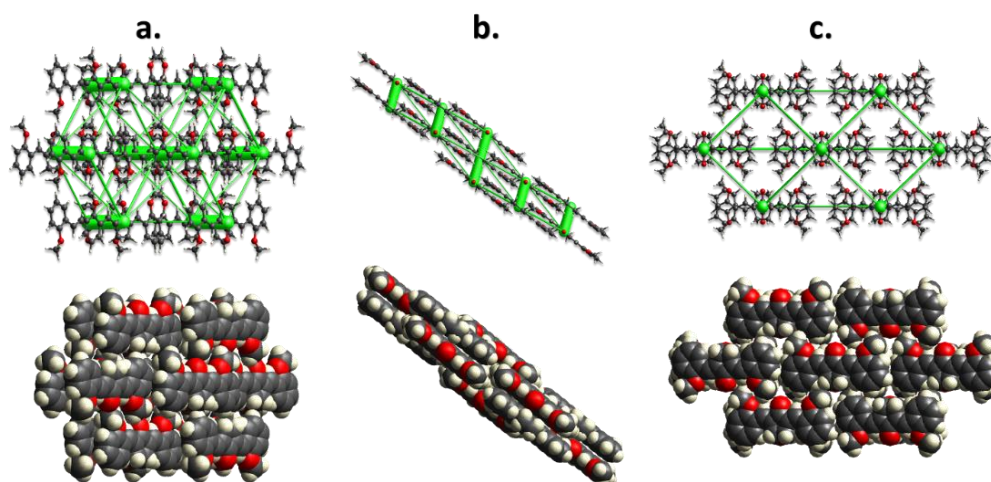


Figure 11. Energy-framework diagrams of E_{dis} for a cluster of molecules. The cylindrical radius is proportional to the relative strength of the corresponding energy and was adjusted to the scale factor of 80 kJ mol^{-1} with a cut-off value of 10 kJ mol^{-1}

3.9. Molecular docking study

A literature review indicates that several investigations have been conducted on drug–DNA interactions. In biological systems, nucleic acids are the primary target molecule. Interactions between molecular compounds and DNA can result in cell DNA damage. Meanwhile, the feasibility of

associating with DNA is always determined by non-covalent interactions, such as electrostatic interactions, complexation, or minor-groove binding. For structure-based drug design, the molecular docking approach is typically used to predict drug–DNA interactions and the binding orientation of the molecule drug. As a result, docking is critical in the rational design of drugs.⁶⁷

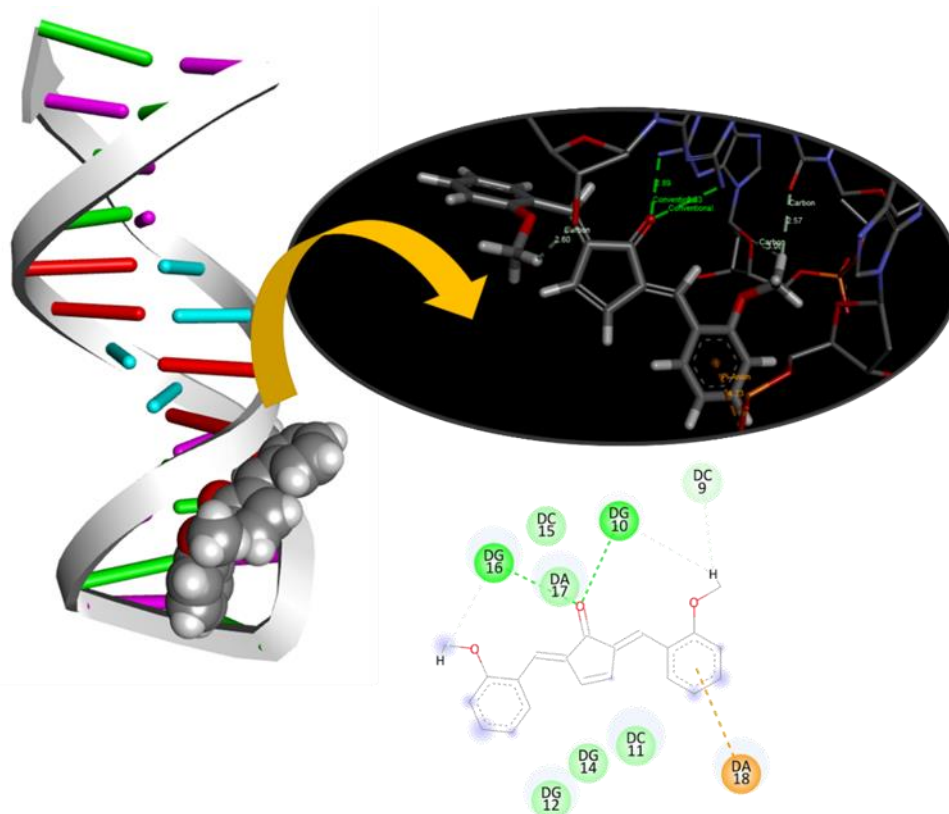


Fig. 12. Molecular docked model of **B2MBCP** with DNA (PDB ID: 1BNA)

The negative binding energies of docked substances indicate that they bind to DNA components. As a result, the binding free energy of the molecule was determined to be -7.8 kcal/mol, indicating a greater capacity to bind. Typically, the geometries of the groove-binding molecules fit the curvature of the grooves. Thus, an ideal binding fit is achieved by interactions such as van der Waals contacts and hydrogen bonding. As seen in Figure 12, the compound is held in place by hydrogen bonds in the minor groove. Additionally, the subsequent docking analysis demonstrates that the title compound binds to DNA (PDB ID: 1BNA) through H-bonds. The $-C=O$ group of the **B2MBCP** interacts with DG16 (2.83 Å) and DG10 (2.83 Å) of the DNA through H-bonds. Two more of these H-bonds take place through the H atoms of the methoxy group of the **B2MBCP** [DG16 (2.60 Å) and DC9 (2.57 Å)]. There is also a π -anion interaction between one of the benzene rings of the **B2MBCP** and the DA(18) moiety of the DNA (4.23 Å). These cooperative interactions are responsible for the intercalation. This intercalation is one of the most important interactions substantial to DNA-binding mechanisms, which may be

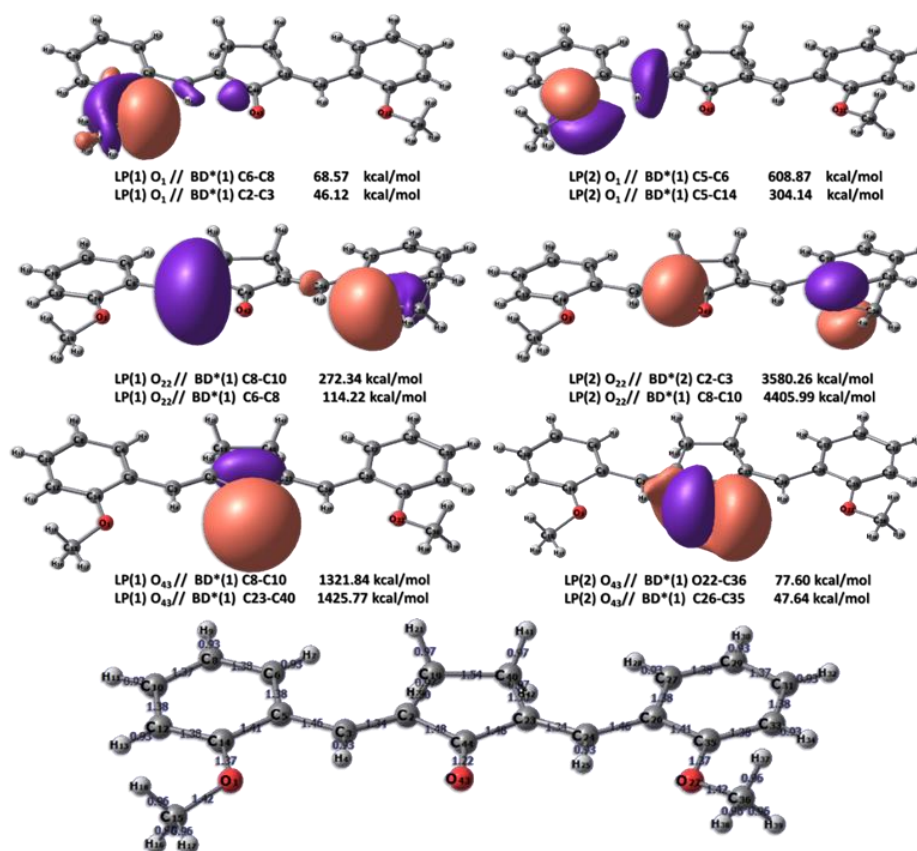
related to some of the compound's biological activity.^{27,68,69}

3.10. Natural bond orbital (NBO) analysis

Natural bond orbital (NBO) analysis can provide an accurate Lewis structure of a molecule by maximizing the electron density of an orbital and, in general, as a sensitive tool for analyzing intra- and intermolecular interactions due to information about filled and virtual orbital interactions.⁷⁰ For each donor (i) and acceptor (j), the stabilization energy $E(2)$ associated with i - j delocalization is estimated as follows:

$$E(2) = \Delta E_{ij} = q_i \frac{F(i,j)^2}{E_j - E_i} \quad (\text{eq. 2})$$

where q_i is the donor orbital occupancy, E_i , E_j is the diagonal elements, and $F(i,j)$ is the off-diagonal NBO Fock matrix element. The stronger the $E(2)$ value, the more intense the contact between donor and acceptor, the greater the inclination of electron donor to acceptor to donate, and the greater the amount of conjugation of the entire system. The NBO analysis of the title compound is presented in Figure 13.



As seen in Figure 13, the whole molecular structure is stabilized to a large extent by the hyperconjugation of the oxygen lone pairs (with different contributions). Significant stability results from hyperconjugation of oxygen's lone pairs with adjacent double-bond carbons in the $-C=O$ group. This interaction transfers electron density to antibonding orbitals, leading to resonance and altering the molecule's reactivity.

3.11. Reduced density gradient (RDG) study

The non-covalent interaction (NCI) surface plot and the reduced density gradient (RDG) vs. λ sign are used to determine the nature of the interaction between the molecules within the crystal structure. The greenish-blueish colored surface and

spikes with negative sign (λ) values in the 2D NCI plot indicate that the generated structures exhibit van der Waals interactions (Fig. 14).

Chemists can quickly identify relevant interactions in a chemical system by graphically illustrating them. Reduced density gradients (RDGs) have been extensively used in the literature to depict weak interaction zones visually. In reality, they may also be used to highlight chemical bonding regions. In this context, the distinctive feature of Tian Lu's interaction region indicator (IRI) is its ability to reveal all types of interactions in a chemical system, including covalent and non-covalent interactions.⁷¹ As seen in Figure 15, the presence of both bonding and Van der Waals interactions are visible in the structure (in line with results from the NCI plot).

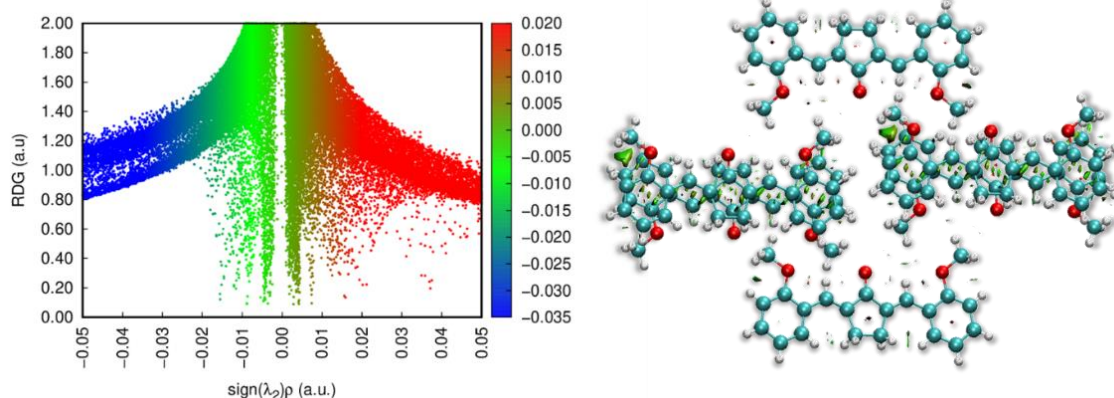


Fig. 14. Non-covalent interaction (NCI) surfaces and the plot of RDG vs sign (λ) ρ for the Van der Waals interactions among packed molecules within the crystal

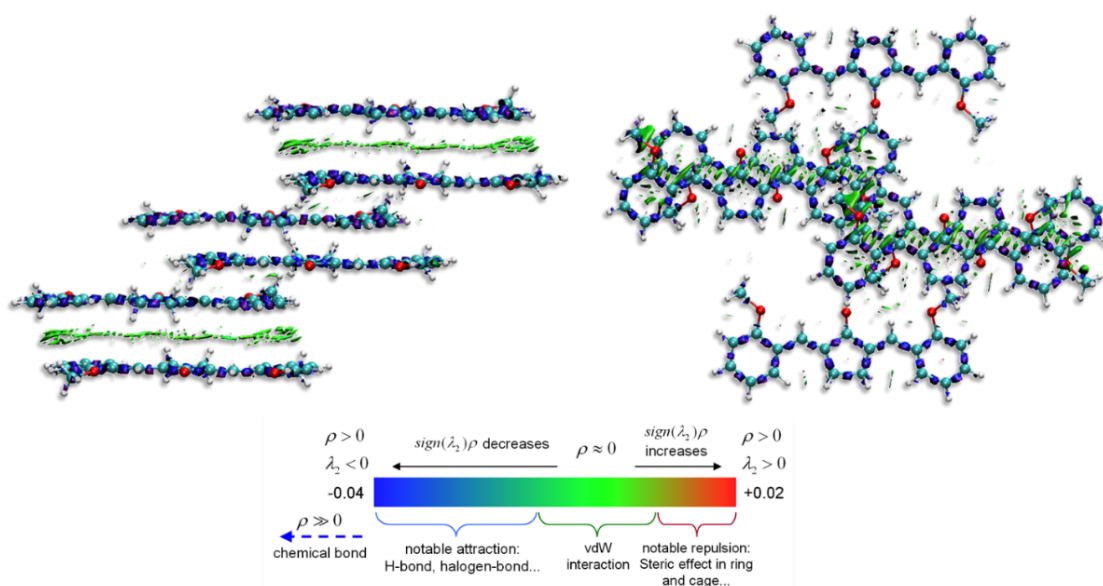


Fig. 15. Interaction region indicator of the packed molecules within the crystal (the bonding and lateral van der Waals interactions are visible in the plot)

3.12. Rotation energy barrier

The dihedral scan from 0 to 360 degrees using a 15-degree step scan for both the molecules in the gas phase is presented in Figure 16. The required energy for complete rotation across a dou-

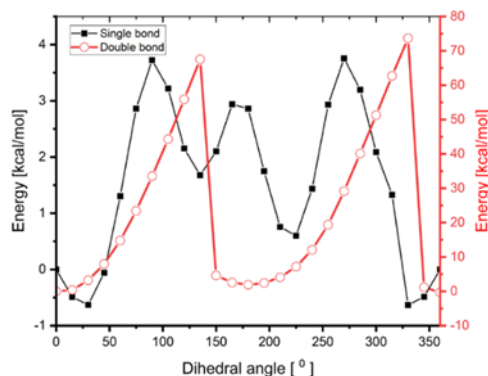


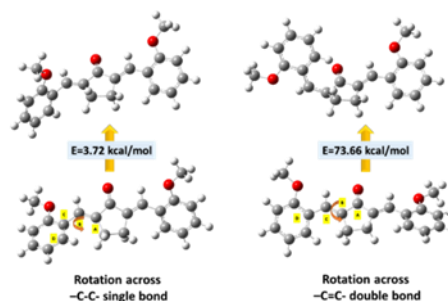
Fig. 16. Calculated rotation barrier across $-C=C$ and $C-C$ for the title compound

4. CONCLUSIONS

The title compound, (2E,5E)-2,5-bis(2-methoxybenzylidene)cyclopentanone, was prepared and spectroscopically characterized (UV-Vis, FT-IR, 1H and ^{13}C NMR). There is good agreement between the experimental and theoretical spectroscopic data. GO adsorption features, as well as an electrochemical study with CV, were performed in this study. Using the DFT calculations, we investigated its molecular structure, absorption properties, molecular docking, rotation barrier, noncovalent interaction surfaces, Hirshfeld surface, and NBO analysis. The rotation barrier study shows that the energy for complete rotation across the double bond is 73.66 kcal/mol, whereas for single bond rotation it is only 3.72 kcal/mol – explaining the flexibility of the side group during the docking study.

The relatively bulky methoxy groups cause a slight increase in the rotation barrier compared to the unsubstituted MAC. The analysis of the crystal structure reveals that the packing of this molecule is dominated by Van der Waals interactions. The NBO analysis shows that the whole molecular structure is stabilized to a large extent by the hyperconjugation of the oxygen lone pairs (with different contributions). Graphene has shown excellent adsorbent properties for B2MBCP through Van der Waals forces and π - π stacking interactions. Exploring additional fluorescent cyclopentanone derivatives for adsorption onto graphene is intriguing, especially when considering the possi-

ble bond is 73.66 kcal/mol. Whereas for single bond rotation, it is only 3.72 kcal/mol. The rotation barrier of the molecule due to the presence of a bulky substituent is higher than the non-substituted derivative, namely (2E,5E)-2,5-dibenzylidene-cyclopentanone.⁷²



bility of investigating their transport through fluorescence analysis within *in vitro* cell membranes. Such research holds the potential to provide valuable insights into drug delivery mechanisms, allowing for direct observation of transport and potential accumulation of the fluorescent graphene-cyclopentanone derivative within cellular organelles.

Acknowledgments. The NMR spectra were recorded at the University of Giessen by Prof. Dr. Siegfried Schindler and with the support of Prof. Dr. Arben Hazi, University of Prishtina.

REFERENCES

- (1) Govindarajan, V. S.; Stahl, W. H., Turmeric — Chemistry, Technology, and Quality. *Critical Reviews in Food Science & Nutrition* **1980**, *12* (3), 199–301. <https://doi.org/10.1080/10408398009527278>
- (2) Fuloria, S.; Mehta, J.; Chandel, A.; Sekar, M.; Rani, N. N. I. M.; Begum, M. Y.; Subramanian, V.; Chidambaram, K.; Thangavelu, L.; Nordin, R.; Wu, Y. S.; Sathasivam, K. V.; Lum, P. T.; Meenakshi, D. U.; Kumarasamy, V.; Azad, A. K.; Fuloria, N. K., A comprehensive review on the therapeutic potential of *Curcuma longa* Linn. in relation to its major active constituent curcumin. *Front. Pharmacol.* **2022**, *13*, 820806. <https://doi.org/10.3389/fphar.2022.820806>
- (3) Salehi, B.; Stojanović-Radić, Z.; Matejić, J.; Sharifi-Rad, M.; Anil Kumar, N. V.; Martins, N.; Sharifi-Rad, J., The therapeutic potential of curcumin: A review of clinical trials. *Eur. J. Med. Chem.* **2019**, *163*, 527–545. <https://doi.org/10.1016/j.ejmech.2018.12.016>
- (4) Ammon, H. P.; Wahl, M. A., Pharmacology of *Curcuma longa*. *Planta Med.* **1991**, *57* (1), 1–7. <https://doi.org/10.1055/s-2006-960004>

- (5) Thangapazham, R. L.; Sharma, A.; Maheshwari, R. K., Multiple molecular targets in cancer chemoprevention by curcumin. *AAPS J.* **2006**, *8* (3), E443-9. <https://doi.org/10.1208/aapsj080352>
- (6) Jayaprakasha, G. K.; Jena, B. S.; Negi, P. S.; Sakariah, K. K., Evaluation of antioxidant activities and antimutagenicity of turmeric oil: A byproduct from curcumin production. *Z. Naturforsch. C* **2002**, *57* (9–10), 828–835. <https://doi.org/10.1515/znc-2002-9-1013>
- (7) Sharma, R. A.; Steward, W. P.; Gescher, A. J., Pharmacokinetics and pharmacodynamics of curcumin. *Adv. Exp. Med. Biol.* **2007**, *595*, 453–470.
- (8) Maheshwari, R. K.; Singh, A. K.; Gaddipati, J.; Srimal, R. C., Multiple biological activities of curcumin: a short review. *Life Sci.* **2006**, *78* (18), 2081–2087.
- (9) Nelson, K. M.; Dahlin, J. L.; Bisson, J.; Graham, J.; Pauli, G. F.; Walters, M. A., The essential medicinal chemistry of curcumin. *J. Med. Chem.* **2017**, *60* (5), 1620–1637. <https://doi.org/10.1021/acs.jmedchem.6b00975>
- (10) Lin, L.; Shi, Q.; Su, C.-Y.; Shih, C. C.-Y.; Lee, K.-H., Antitumor agents 247. New 4-ethoxycarbonylethyl curcumin analogs as potential antiandrogenic agents. *Bioorg. Med. Chem.* **2006**, *14* (8), 2527–2534. <https://doi.org/10.1016/j.bmc.2005.11.034>
- (11) Dimmock, J. R.; Padmanilayam, M. P.; Zello, G. A.; Nienaber, K. H.; Allen, T. M.; Santos, C. L.; De Clercq, E.; Balzarini, J.; Manavathu, E. K.; Stables, J. P., Cytotoxic analogues of 2,6-bis(arylidene)cyclohexanones. *Eur. J. Med. Chem.* **2003**, *38* (2), 169–177.
- (12) Liang, G.; Yang, S. L.; Shao, L. L.; Zhao, C. G.; Xiao, J.; Lv, Y. X.; Yang, J.; Zhao, Y.; Li, X. K., Synthesis, structure, and bioevaluation of 2,5-bis(arylmethenyl)cyclopentanones. *Journal of Asian Natural Products Research* **2008**, *10* (10), 957–965. <https://doi.org/10.1080/10286020802181257>
- (13) Zhao, C.; Liu, Z.; Liang, G., Promising curcumin-based drug design: mono-carbonyl analogues of curcumin (MACs). *Curr. Pharm. Des.* **2013**, *19* (11), 2114–2135.
- (14) Shetty, D.; Kim, Y. J.; Shim, H.; Snyder, J. P., Eliminating the heart from the curcumin molecule: monocarbonyl curcumin mimics (MACs). *Molecules* **2014**, *20* (1), 249–292. <https://doi.org/10.3390/molecules20010249>
- (15) Liang, G.; Shao, L.; Wang, Y.; Zhao, C.; Chu, Y.; Xiao, J.; Zhao, Y.; Li, X.; Yang, S., Exploration and synthesis of curcumin analogues with improved structural stability both in vitro and in vivo as cytotoxic agents. *Bioorganic and Medicinal Chemistry* **2009**, *17* (6), 2623–2631.
- (16) Hadzi-Petrushev, N.; Bogdanov, J.; Krajoska, J.; Ilievska, J.; Bogdanova-Popov, B.; Gjorgievska, E.; Mitrokhin, V.; Sopi, R.; Gagov, H.; Kamkin, A.; Mladenov, M., Comparative study of the antioxidant properties of monocarbonyl curcumin analogues C66 and B2BrBC in isoproterenol induced cardiac damage. *Life Sci.* **2018**, *197*, 10–18. <https://doi.org/10.1016/j.lfs.2018.01.028>
- (17) Stamenkovska, M.; Hadzi-Petrushev, N.; Nikodinovski, A.; Gagov, H.; Atanasova-Panchevska, N.; Mitrokhin, V.; Kamkin, A.; Mladenov, M., application of curcumin and its derivatives in the treatment of cardiovascular diseases: A review. *Int. J. Food Prop.* **2021**, *24* (1), 1510–1528. <https://doi.org/10.1080/10942912.2021.1977655>
- (18) Stojchevski, R.; Angelovski, M.; Velichkovikj, S.; Hadzi-Petrushev, N.; Mladenov, M.; Bogdanov, J. B.; Poretsky, L.; Avtanski, D., 557-P: Effect of monocarbonyl curcumin analogues C66 and B2BrBC on pancreatic expression of genes related to insulin signaling pathway and oxidative stress in streptozotocin-induced diabetes, June 3–7 2022. https://diabetesjournals.org/diabetes/article/71/Supplement_1/557-P/146211
- (19) Todorovska, I.; Dragarska, K.; Bogdanov, J., A combined 2D- and 3D-QSAR study, design and synthesis of some monocarbonyl curcumin analogs as potential inhibitors of MDA-MB-231 breast cancer cells. *Chem. Proc.* **2022**, *12* (1), 5. <https://doi.org/10.3390/ecsoc-26-13572>
- (20) Lozanovski, Z.; Petreska-Stanoeva, J.; Bogdanov, J., Development of a spectrophotometric method for assessment of the relative reactivity of monocarbonyl analogs of curcumin with 2-(dimethylamino)ethanethiol. *Maced. J. Chem. Chem. Eng.* **2023**, *42* (1), 13–24. <https://doi.org/10.20450/mjccce.2023.2638>
- (21) Zamrus, S. N. H.; Akhtar, M. N.; Yeap, S. K.; Quah, C. K.; Loh, W. S.; Alitheen, N. B.; Zareen, S.; Tajuddin, S. N.; Hussin, Y.; Shah, S. A. A., Design, synthesis and cytotoxic effects of curcuminoids on HeLa, K562, MCF-7 and MDA-MB-231 cancer cell lines. *Chem. Cent. J.* **2018**, *12* (1), 31.
- (22) Zoete, V.; Rougée, M.; Dinkova-Kostova, A. T.; Talalay, P.; Bensasson, R. V., Redox ranking of inducers of a cancer-protective enzyme via the energy of their highest occupied molecular orbital. *Free Radic. Biol. Med.* **2004**, *36* (11), 1418–1423. <https://doi.org/10.1016/j.freeradbiomed.2004.03.008>
- (23) Vatsadze, S. Z.; Gavrilova, G. V.; Zyuz'kevich, F. S.; Nuriev, V. N.; Krut'ko, D. P.; Moiseeva, A. A.; Shumyantsev, A. V.; Vedernikov, A. I.; Churakov, A. V.; Kuz'mina, L. G.; Howard, J. A. K.; Gromov, S. P., Synthesis, structure, electrochemistry, and photophysics of 2,5-dibenzylidenecyclopentanones containing in benzene rings substituents different in polarity. *Russ. Chem. Bull.* **2016**, *65* (7), 1761–1772.
- (24) De Assis, L. K.; Damasceno, B. S.; Carvalho, M. N.; Oliveira, E. H. C.; Ghislandi, M. G., Adsorption capacity comparison between graphene oxide and graphene nanoplatelets for the removal of coloured textile dyes from wastewater. *Environ. Technol.* **2020**, *41* (18), 2360–2371. <https://doi.org/10.1080/09593330.2019.1567603>
- (25) Kini, S. G.; Choudhary, S.; Mubeen, M., Synthesis, docking study and anticancer activity of coumarin substituted derivatives of benzothiazole. **2012**, *2* (1), 51–60.
- (26) Sastry, S. S. M.; Panjekar, S.; Raman, R. K. S. Graphene and Graphene Oxide as a Support for Biomolecules in the Development of Biosensors. *Nanotechnology, Science and Applications* **2021**, *14* (October), 197–220. <https://doi.org/10.2147/NSA.S334487>
- (27) Huber, I.; Rozmer, Z.; Gyöngyi, Z.; Budán, F.; Horváth, P.; Kiss, E.; Perjési, P., structure activity relationship analysis of antiproliferative cyclic C5-curcuminoids

- without DNA binding: design, synthesis, lipophilicity and biological activity. *J. Mol. Struct.* **2020**, *1206*, 127661. <https://doi.org/10.1016/j.molstruc.2019.127661>
- (28) Zhao, C.-G.; Yang, J.; Huang, Y.; Liang, G.; Li, X.-K., Crystal structure of ortho-(2E,5E)-2,5-bis(2-methoxybenzylidene) cyclopentanone, C₂₁H₂₀O₃. *Kristallogr. - New Cryst. Struct.* **2009**, *224* (2), 337–338.
- (29) Weber, W. M.; Hunsaker, L. A.; Abcouwer, S. F.; Deck, L. M.; Vander Jagt, D. L., Anti-oxidant activities of curcumin and related enones. *Bioorg. Med. Chem.* **2005**, *13* (11), 3811–3820. <https://doi.org/10.1016/j.bmc.2005.03.035>
- (30) Tirado-Rives, J.; Jorgensen, W. L., Performance of B3LYP density functional methods for a large set of organic molecules. *J. Chem. Theory Comput.* **2008**, *4* (2), 297–306. <https://doi.org/10.1021/ct700248k>
- (31) Zheng, D.; Zhang, M.; Zhao, G., Combined TDDFT and AIM insights into photoinduced excited state intramolecular proton transfer (ESIPT) mechanism in hydroxyl-and amino-anthraquinone solution. *Scientific Reports* **2017**, *7* (1), 1–10. <https://doi.org/10.1038/s41598-017-14094-5>
- (32) Li, Y.; Chu, T.-S. DFT/TDDFT Study on the sensing mechanism of a fluorescent probe for hydrogen sulfide: excited state intramolecular proton transfer coupled twisted intramolecular charge transfer. *J. Phys. Chem. A* **2017**, *121* (28), 5245–5256. <https://doi.org/10.1021/acs.jpca.7b02606>
- (33) Berisha, A., Interactions between the aryldiazonium cations and graphene oxide: A DFT study. *J. Chem. Chem. Eng.* **2019**, *2019*. <https://doi.org/10.1155/2019/5126071>
- (34) Berisha, A.; Combellas, C.; Kanoufi, F.; Médard, J.; Decorse, P.; Mangeney, C.; Kherbouche, I.; Seydou, M.; Maurel, F.; Pinson, J., Alkyl-modified gold surfaces: characterization of the Au-C bond. *Langmuir* **2018**, *34* (38), 11264–11271. <https://doi.org/10.1021/acs.langmuir.8b01584>
- (35) Lu, T.; Chen, F. Multiwfn: A., Multifunctional wavefunction analyzer. *J. Comput. Chem.* **2012**, *33* (5), 580–592. <https://doi.org/10.1002/jcc.22885>
- (36) Yamada, Y.; Gohda, S.; Abe, K.; Togo, T.; Shimano, N.; Sasaki, T.; Tanaka, H.; Ono, H.; Ohba, T.; Kubo, S.; Ohkubo, T.; Sato, S., Carbon materials with controlled edge structures. *Carbon N. Y.* **2017**, *122*, 694–701. <https://doi.org/10.1016/j.carbon.2017.07.012>
- (37) Humphrey, W.; Dalke, A.; Schulten, K., VMD: Visual molecular dynamics. *J. Mol. Graph.* **1996**, *14* (1), 33–38, 27–28. [https://doi.org/10.1016/0263-7855\(96\)00018-5](https://doi.org/10.1016/0263-7855(96)00018-5)
- (38) Hourahine, B.; Aradi, B.; Blum, V.; Bonafé, F.; Buccheri, A.; Camacho, C.; Cevallos, C.; Deshayé, M. Y.; Dumitrică, T.; Dominguez, A.; Ehlert, S.; Elstner, M.; Van der Heide, T.; Hermann, J.; Irle, S.; Kranz, J. J.; Köhler, C.; Kowalczyk, T.; Kubař, T.; Lee, I. S.; Lutsker, V.; Maurer, R. J.; Min, S. K.; Mitchell, I.; Negre, C.; Niehaus, T. A.; Niklasson, A. M. N.; Page, A. J.; Pecchia, A.; Penazzi, G.; Persson, M. P.; Rezáč, J.; Sánchez, C. G.; Sternberg, M.; Stöhr, M.; Stuckenberg, F.; Tkatchenko, A.; Yu, V. W.-Z.; Frauenheim, T., DFTB+, a software package for efficient approximate density functional theory based atomistic simulations. *J. Chem. Phys.* **2020**, *152* (12), 124101. <https://doi.org/10.1063/1.5143190>
- (39) Hamed, R.; Jodeh, S.; Hanbali, G.; Safi, Z.; Berisha, A.; Xhaxhiu, K.; Dagdag, O., Eco-friendly synthesis and characterization of double-crossed link 3d graphene oxide functionalized with chitosan for adsorption of sulfamethazine from aqueous solution: Experimental and DFT calculations. *Front. Environ. Sci. Eng. China* **2022**, *10*. <https://doi.org/10.3389/fenvs.2022.930693>
- (40) Sundaraganesan, N.; Joshua, B. D.; Radjakoumar, T., Molecular structure and vibrational spectra of 2-chlorobenzoic acid by density functional theory and ab-initio Hartree-Fock calculations. *Indian J. Pure Appl. Phys.* **2009**.
- (41) Saleem, H.; Krishnan, A. R.; Erdogdu, Y.; Subashchandrabose, S.; Thanikachalam, V.; Manikandan, G., Density Functional theory studies on 2,5-bis(4-hydroxy-3-methoxybenzylidene)cyclopentanone. *J. Mol. Struct.* **2011**, *999* (1), 2–9. <https://doi.org/10.1016/j.molstruc.2011.02.039>
- (42) Sajan, D.; Udaya Lakshmi, K.; Erdogdu, Y.; Hubert Joe, I., Molecular structure and vibrational spectra of 2,6-bis(benzylidene)cyclohexanone: A density functional theoretical study. *Spectrochim. Acta A Mol. Biomol. Spectrosc.* **2011**, *78* (1), 113–121. <https://doi.org/10.1016/j.saa.2010.09.007>
- (43) George, J.; Thomas, A. K.; Sajan, D.; Sathiyamoorthi, S.; Srinivasan, P.; Joy, N.; Philip, R., Experimental and DFT/TD-DFT approach on photo-physical and NLO properties of 2, 6-bis (4-chlorobenzylidene) cyclohexanone. *Opt. Mater.* **2020**, *100*, 109620. <https://doi.org/10.1016/j.optmat.2019.109620>
- (44) *Organic Electrochemistry*, Hammerich, O., Lund, H., Eds.; 4th edition revised and expanded; Marcel Dekker, Inc.: New York, NY, 2000.
- (45) Fomina, M. V.; Vatsadze, S. Z.; Freidzon, A. Y.; Kuz'mina, L. G.; Moiseeva, A. A.; Starostin, R. O.; Nuriev, V. N.; Gromov, S. P., Structure–property relationships of dibenzylidenecyclohexanones. *ACS Omega* **2022**, *7* (12), 10087–10099. <https://doi.org/10.1021/acsomega.1c06129>
- (46) Abdolhosseinzadeh, S.; Asgharzadeh, H.; Seop Kim, H., Fast and fully-scalable synthesis of reduced graphene oxide. *Sci. Rep.* **2015**, *5*, 10160. <https://doi.org/10.1038/srep10160>
- (47) Thakur, K.; Kandasubramanian, B., Graphene and graphene oxide-based composites for removal of organic pollutants: A review. *J. Chem. Eng. Data* **2019**, *64* (3), 833–867. <https://doi.org/10.1021/acs.jced.8b01057>
- (48) Zhu, X.; Tsang, D. C. W.; Chen, F.; Li, S.; Yang, X., Ciprofloxacin adsorption on graphene and granular activated carbon: kinetics, isotherms, and effects of solution chemistry. *Environ. Technol.* **2015**, *36* (24), 3094–3102. <https://doi.org/10.1080/09593330.2015.1054316>
- (49) Mehmeti, V.; Halili, J.; Berisha, A., Which is better for lindane pesticide adsorption, graphene or graphene oxide? An experimental and DFT study. *J. Mol. Liq.* **2022**, *347*, 118345. <https://doi.org/10.1016/j.molliq.2021.118345>

- (50) Aradi, B.; Hourahine, B.; Frauenheim, T., DFTB+, a sparse matrix-based implementation of the DFTB method. *J. Phys. Chem. A* **2007**, *111* (26), 5678–5684. <https://doi.org/10.1021/jp070186p>
- (51) Hourahine, B.; Sanna, S.; Aradi, B.; Köhler, C.; Niehaus, T.; Frauenheim, T., Self-interaction and strong correlation in DFTB. *J. Phys. Chem. A* **2007**, *111* (26), 5671–5677. <https://doi.org/10.1021/jp070173b>
- (52) Berisha, A., First principles details into the grafting of aryl radicals onto the free-standing and borophene/Ag(1 1 1) surfaces. *Chemical Physics* **2021**, *544* (January), 111124. <https://doi.org/10.1016/j.chemphys.2s21.111124>
- (53) Mehmeti, V.; Sadiku, M., A comprehensive DFT investigation of the adsorption of polycyclic aromatic hydrocarbons onto graphene. *Computation* **2022**, *10* (5), 68. <https://doi.org/10.3390/computation10050068>
- (54) Fujimoto, H.; Fukui, K., Molecular orbital theory of chemical reactions. *Advances in Quantum Chemistry* **1972**, *6* (C), 177–201. [https://doi.org/10.1016/S0065-3276\(08\)60545-6](https://doi.org/10.1016/S0065-3276(08)60545-6)
- (55) Woodward, R. B.; Hoffmann, R., The Conservation of orbital symmetry. *Angew. Chem. Int. Ed Engl.* **1969**, *8* (11), 781–853. <https://doi.org/10.1002/anie.196907811>
- (56) Pandya, S. B.; Patel, U. H.; Chaudhary, K. P.; Socha, B. N.; Patel, N. J.; Bhatt, B. S., DNA interaction, cytotoxicity and molecular structure of cobalt complex of 4-amino-n-(6-chloropyridazin-3-yl)benzene sulfonamide in the presence of secondary ligand pyridine. *Applied Organometallic Chemistry* **2019**, *33* (12), 1–14. <https://doi.org/10.1002/aoc.5235>
- (57) Manne, R.; Åberg, T., Koopmans' theorem for inner-shell ionization. *Chem. Phys. Lett.* **1970**, *7* (2), 282–284. [https://doi.org/10.1016/0009-2614\(70\)80309-8](https://doi.org/10.1016/0009-2614(70)80309-8)
- (58) Dubey, R. P.; Patel, U. H.; Tailor, S. M., DFT studies, hirshfeld surface analysis and crystal structure of novel silver complex of sulfapyridine with secondary ligand pyridine. *Mol. Cryst. Liq. Cryst.* **2017**, *656* (1), 139–152. <https://doi.org/10.1080/15421406.2017.1397432>
- (59) McKinnon, J. J.; Jayatilaka, D.; Spackman, M. A., Towards quantitative analysis of intermolecular interactions with Hirshfeld surfaces. *Chem. Commun.* **2007**, No. 37, 3814–3816. <https://doi.org/10.1039/b704980c>
- (60) Spackman, M. A.; Jayatilaka, D., Hirshfeld surface analysis. *CrystEngComm* **2009**, *11* (1), 19–32. <https://doi.org/10.1039/b818330a>
- (61) Wood, P. A.; McKinnon, J. J.; Parsons, S.; Pidcock, E.; Spackman, M. A., Analysis of the compression of molecular crystal structures using Hirshfeld surfaces. *CrystEngComm* **2008**, *10* (4), 368–376. <https://doi.org/10.1039/b715494a>
- (62) Mohamooda Sumaya, U.; KarunaKaran, J.; Biruntha, K.; MohanaKrishnan, A. K.; Usha, G., Crystal structure and Hirshfeld surface analysis and energy frameworks of 1-(2,4-dimethylphenyl)-4-(4-methoxyphenyl)naphthalene. *Acta Crystallographica Section E: Crystallographic Communications* **2018**, *74* (15), 939–943. <https://doi.org/10.1107/S2056989018008332>
- (63) Koenderink, J. J.; Van Doorn, A. J., Surface shape and curvature scales. *Image Vis. Comput.* **1992**, *10* (8), 557–564. [https://doi.org/10.1016/0262-8856\(92\)90076-F](https://doi.org/10.1016/0262-8856(92)90076-F)
- (64) Tan, S. L.; Jotani, M. M.; Tiekink, E. R. T., Utilizing Hirshfeld surface calculations, non-covalent interaction (NCI) Plots and the calculation of interaction energies in the analysis of molecular packing. *Acta Crystallographica Section E: Crystallographic Communications* **2019**, *75*, 308–318. <https://doi.org/10.1107/S2056989019001129>
- (65) Mackenzie, C. F.; Spackman, P. R.; Jayatilaka, D.; Spackman, M. A., CrystalExplorer model energies and energy frameworks: extension to metal coordination compounds, organic salts, solvates and open-shell systems. *IUCrJ* **2017**, *4*, 575–587. <https://doi.org/10.1107/S205225251700848X>
- (66) Patel, M. K.; Patel, U. H.; Gandhi, S. A.; Barot, V. M.; Jayswal, J., Solvent effect on neutral Co (II) complexes of paeonol derivative—qualitative and quantitative studies from energy frame work and Hirshfeld surface analysis. *J. Mol. Struct.* **2019**, *1196*, 119–131. <https://doi.org/10.1016/j.molstruc.2019.06.050>
- (67) Chandraleka, S.; Ramya, K.; Chandramohan, G.; Dhanasekaran, D.; Priyadarshini, A.; Panneerselvam, A., Antimicrobial mechanism of copper (II) 1,10-phenanthroline and 2,2'-bipyridyl complex on bacterial and fungal pathogens. *Journal of Saudi Chemical Society* **2014**, *18* (6), 953–962. <https://doi.org/10.1016/j.jscs.2011.11.020>
- (68) Bholra, Y. O.; Socha, B. N.; Pandya, S. B.; Dubey, R. P.; Patel, M. K., Molecular structure, DFT studies, Hirshfeld surface analysis, energy frameworks, and molecular docking studies of novel (E)-1-(4-chlorophenyl)-5-methyl-N'-((3-methyl-5-phenoxy-1-phenyl-1H-pyrazol-4-yl) methylene)-1H-1, 2, 3-triazole-4-carbohydrazide. *Mol. Cryst. Liq. Cryst.* **2019**, *692* (1), 83–93. <https://doi.org/10.1080/15421406.2020.1721946>
- (69) Göktürk, T.; Sakallı Çetin, E.; Hökelek, T.; Pekel, H.; Şensoy, Ö.; Aksu, E. N.; Güp, R., Synthesis, structural investigations, DNA/BSA interactions, molecular docking studies, and anticancer activity of a new 1,4-disubstituted 1,2,3-triazole derivative. *ACS Omega* **2023**, *8* (35), 31839–31856. <https://doi.org/10.1021/acsoomega.3c03355>
- (70) Li, L.; Wu, C.; Wang, Z.; Zhao, L.; Li, Z.; Sun, C.; Sun, T., Density functional theory (DFT) and natural bond orbital (NBO) study of vibrational spectra and intramolecular hydrogen bond interaction of l-ornithine-l-aspartate. *Spectrochimica Acta - Part A: Molecular and Biomolecular Spectroscopy* **2015**, *136* (PB), 338–346. <https://doi.org/10.1016/j.saa.2014.08.153>
- (71) Lu, T.; Chen, Q., Interaction region indicator: A simple real space function clearly revealing both chemical bonds and weak interactions. *Chem. Methods* **2021**, *1* (5), 231–239. <https://doi.org/10.1002/cmt.202100007>
- (72) Thaçi, V.; Hoti, R.; Berisha, A.; Bogdanov, J., Corrosion study of copper in aqueous sulfuric acid solution in the presence of (2E,5E)-2,5-dibenzylidenecyclopentanone and (2E,5E)-Bis[(4-dimethylamino)benzylidene]cyclopentanone: Experimental and Theoretical Study. *Open Chem.* **2020**, *18* (1), 1412–1420. <https://doi.org/10.1515/chem-2020-0172>